nature communications

Article

https://doi.org/10.1038/s41467-025-58419-9

Synthesis of nickel(II)-containing *meso*-edited phthalocyanine derivatives

Received: 19 September 2024

Accepted: 20 March 2025

Published online: 29 March 2025

Check for updates

Yuta Takiya[1], Taiga Saito[1], Naoyuki Toriumi[1] ✉ & Masanobu Uchiyama[1,2] ✉

In contrast to the rich chemistry of porphyrin and its analogs, the structural variety of phthalocyanine derivatives, which are widely utilized in material and life sciences, has been limited by the lack of versatile synthetic methods. Herein we present a synthetic strategy/methodology for the *meso*-position editing of phthalocyanine derivatives via deprotonative macrocyclization of open-form acyclic phthalonitrile Ni tetramer **1**, prepared by thiolate-mediated reductive tetramerization of phthalonitrile and metalation. To illustrate the utility of this protocol, we synthesize several *meso*-*N*-edited phthalocyanine derivatives, including 16π-electron antiaromatic tetrabenzodiazanorcorrole **2**, and 17π-electron paramagnetic tetrabenzotriazacorrole **3** and tetrabenzodiazacorrole **4**. The products are obtained as the nickel(II) complexes. Their unique electronic properties, such as paratropicity and radical character, are characterized both experimentally and computationally. Moreover, antiaromatic compound **2** undergoes further *meso*-position and skeletal transformations upon reaction with nucleophiles to give nonaromatic and aromatic π-conjugates.

Porphyrinoids are an important class of cyclic π-conjugated aromatic molecules that are of synthetic, theoretical, and applicational interest. Among them, phthalocyanine, which is composed of four isoindoline units with bridging *meso*-nitrogen (*N*) atoms, exhibits outstanding physicochemical properties, such as intense absorption/emission in the visible-near-IR region and high electron-accepting ability. Consequently, phthalocyanine derivatives are widely utilized in material and life sciences as functional organic dyes[1–8]. However, the preparation of phthalocyanine and its derivatives has mostly been limited to one-step condensation of isoindolinic equivalents such as phthalonitrile and 1,3-diiminoisoindoline (Fig. 1a)[1,4,5]. The lack of versatile synthetic methods, especially for modification of the *meso*-positions that are critical for the functionality of phthalocyanine derivatives, greatly restricts the structural variety of phthalocyanine derivatives compared with porphyrin derivatives, which can be obtained in a stepwise manner using various combinations of pyrroles and aldehydes[9–12]. Therefore, there is a need for new intermediates and methodologies to access a wider range of phthalocyanine derivatives.

In 2015, Kobayashi and Furuyama et al. discovered the dimerization reaction of phthalonitriles using Na and dodecanethiol at high temperature, obtaining the β-diaminoisoindigo skeleton as the main product (Fig. 1b)[13]. This reaction has been elegantly utilized for the synthesis of a 20π-electron antiaromatic ring-expanded phthalocyanine analogs. This dimerization protocol was also applied to the development of various β-isoindigo dyes[14,15]. Notably, trimerization, tetramerization, and hexamerization of phthalonitriles have also been achieved by the use of sulfur reagents[16,17]. However, despite these pioneering examples, the use of acyclic phthalonitrile oligomers as precursors of phthalocyanine-like macrocycles is still limited due to their unfavorable linear conformation, which makes cyclization difficult.

Here we report an approach to the synthesis of *meso*-edited phthalocyanine derivatives using the folded phthalonitrile Ni tetramer **1** as a synthetic platform (Fig. 1c). **1** was prepared by Ni complexation of the linear phthalonitrile tetramer **5**, which was synthesized via thiolate-mediated oligomerization of phthalonitrile. The configurational transformation induced by complexation was the key to success in the

[1]Graduate School of Pharmaceutical Sciences, The University of Tokyo, Bunkyo-ku, Tokyo, Japan. [2]Research Initiative for Supra-Materials (RISM), Shinshu University, Nagano, Japan. ✉e-mail: toriumi@mol.f.u-tokyo.ac.jp; uchiyama@mol.f.u-tokyo.ac.jp

https://doi.org/10.1038/s41467-025-58419-9

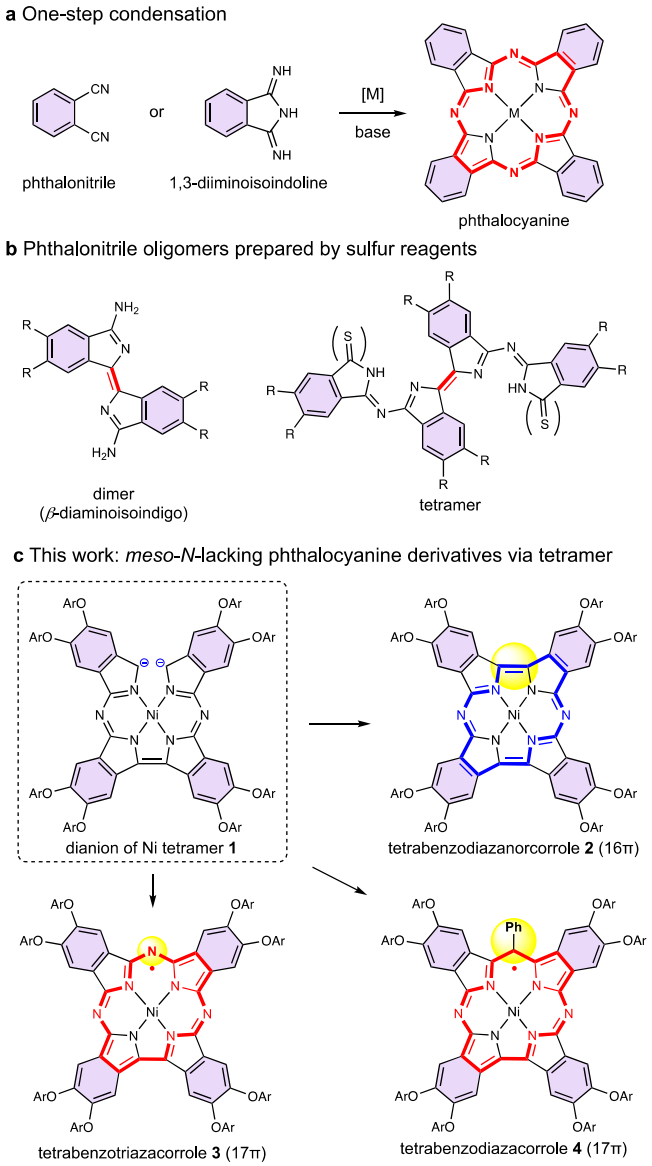

Fig. 1 | Synthesis of phthalocyanine derivatives. a One-step condensation to synthesize phthalocyanine. **b** Examples of phthalonitrile oligomers prepared by sulfur reagents. **c** This work: synthesis of *meso*-*N*-lacking phthalocyanine derivatives as their Ni(II) complexes via tetramer.

following cyclization. The folded tetramer **1** reacts with various electrophiles at the terminal benzylic positions in the presence of a strong base to give stable phthalocyanine-like macrocycles as the nickel(II) complexes. To illustrate the value of this protocol, we employed it for the synthesis of 16π-electron antiaromatic tetrabenzodiazanorcorrole **2**, and 17π-electron paramagnetic tetrabenzotriazacorrole **3** and tetrabenzodiazacorrole **4**. The electronic properties of these compounds were investigated in detail by both experimental and computational methods. Furthermore, we showed that the high electrophilicity of antiaromatic macrocycle **2** could be utilized for *meso*-editing.

Results

Synthesis of macrocycles

Our study commenced with re-optimization of the reaction conditions for the thiolate-mediated reductive oligomerization reaction[16]. The original procedure afforded the tetramer **5** in low yield (<10%) from 4,5-bis(2,6-diisopropylphenoxy)phthalonitrile (**6**) in the presence of Na and dodecanethiol. After extensive experimentation (Supplementary Table 1), we found that the use of bases with larger counter cations, such as K and Cs, led to the selective formation of **5** over the corresponding phthalocyanine; this is consistent with the report that small alkali metal ions such as Li and Na accelerate the formation of phthalocyanine via a metal template effect[5]. Finally, the yield of **5** was increased to 35% by using Cs_2CO_3 as a base. Although the reaction mechanism remains unclear, the thiolate anion seems to work as a reducing agent. The optimized synthetic route towards *meso*-position-modified phthalocyanine derivatives **2**, **3**, and **4** from **5** is shown in Fig. 2. All initial attempts to cyclize **5** directly under various conditions were unsuccessful. We anticipated that configurational transformation to fold the tetramer **5** appropriately by using a metal template would assist the cyclization. Ni was chosen as the central metal due to its strong binding ability and relatively small covalent radius[18]. Complexation of **5** with $Ni(OAc)_2$ proceeded in high yield to afford the open-form folded tetraisoindolinic Ni complex **1**, whose structure was elucidated by single-crystal X-ray diffraction analysis (Supplementary Fig. 13). The isoindoline units at the two ends were placed close to each other as a result of the coordination of Ni. Treatment of **1** with sodium hexamethyldisilazide (NaHMDS) followed by the addition of D_2O resulted in ca. 50% deuterium incorporation at the four protons in the benzylic positions, suggesting in-situ generation of a dianion species (Supplementary Fig. 8). This prompted us to screen various electrophiles for macrocyclization (Fig. 2). Successive treatment of **1** with $PtCl_2$ and NaHMDS led to facile ring closure to give tetrabenzodiazanorcorrole **2**, which lacks two *meso*-*N* atoms of phthalocyanine, in 94% yield. The reaction with *N*-iodosuccinimide (NIS) also gave **2**, albeit in lower yield (25%) (Supplementary Fig. 6). **2** is a rare example of tetrabenzodiazanorcorrole, in contrast to the rich chemistry of 16π-electron antiaromatic norcorrole[19–22]. Next, ring closure with single atom insertion was investigated. The reaction of the dianion with isoamyl nitrate (^{i}AmONO) as an electrophile gave a nitrogen-inserted macrocycle, tetrabenzotriazacorrole **3**[23–25], while the reaction with benzoyl chloride as an electrophile afforded a carbon-inserted macrocycle, tetrabenzodiazacorrole **4**. The high yields of *meso*-modified phthalocyanine derivatives **2**, **3**, and **4** from **5** demonstrate the utility of our successive Ni-complexation and deprotonative functionalization methodology. It is also noteworthy that the macrocycles **2**, **3**, and **4** were bench-stable as solids for at least 6 months in air at room temperature, even though **2** is antiaromatic and **3** and **4** exist as π-radical species, as discussed later.

Physicochemical properties

The structures of macrocycles **2, 3**, and **4** were unambiguously confirmed by single-crystal X-ray diffraction analysis (Fig. 3). The tetrabenzoazaporphyrinoid skeletons of **2, 3**, and **4** take almost planar structures in the solid state; the mean deviations from the averaged planes are 0.052 Å, 0.055 Å, and 0.058 Å, respectively. **2** displays significant bond length alternation in the pyrrole units compared with 18π-electron aromatic Ni phthalocyanine[26], suggesting the presence of 16π-electron antiaromaticity (Supplementary Fig. 19).

To investigate the electronic structures in solution, we measured the ^{1}H NMR spectra of **1, 2, 3**, and **4**. Firstly, to investigate the antiaromaticity of **2** in solution, we compared the ^{1}H NMR spectra of **1** and **2** in $CDCl_3$ at room temperature (Fig. 4a, b). The α protons H^a and H^b of 16π-electron macrocycle **2** were observed at 5.66 and 5.56 ppm, being shifted significantly upfield compared with those of nonaromatic, open-form tetramer **1** at 7.01–6.53 ppm. The aryloxy protons of **2** (7.11–7.00 ppm) were also observed slightly upfield compared with the protons of **1** (7.38–7.09 ppm). These chemical shifts strongly suggest the existence of an antiaromatic paratropic ring current in **2**. The antiaromaticity of **2** was further confirmed by nucleus-independent chemical shifts (NICS)[27] calculation of Ni tetrabenzodiazanorcorrole **2'** without any peripheral substituents (Supplementary Fig. 28). The NICS(1) values inside the macrocycle

https://doi.org/10.1038/s41467-025-58419-9

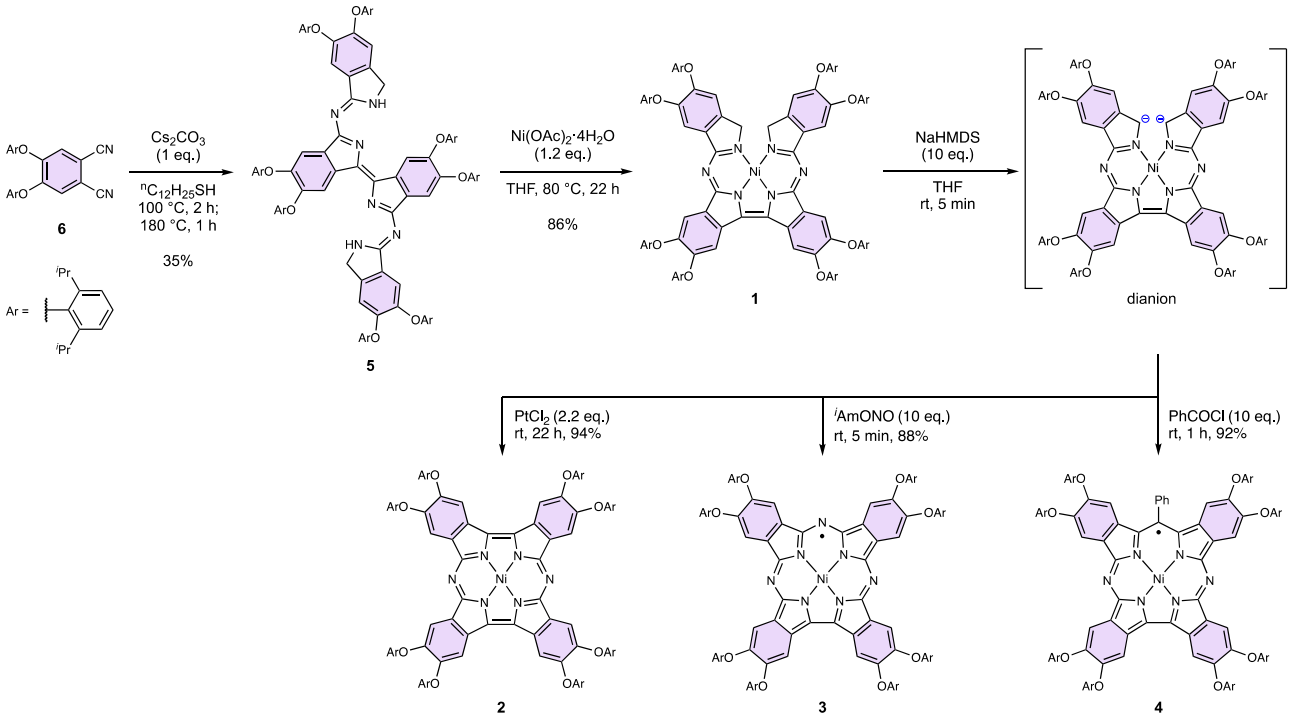

Fig. 2 | Synthesis of Ni(II) complexes of *meso*-edited phthalocyanine derivatives 2, 3, and 4 via open-form Ni tetramer 1. NaHMDS sodium hexamethyldisilazide, ^{i}Am isoamyl.

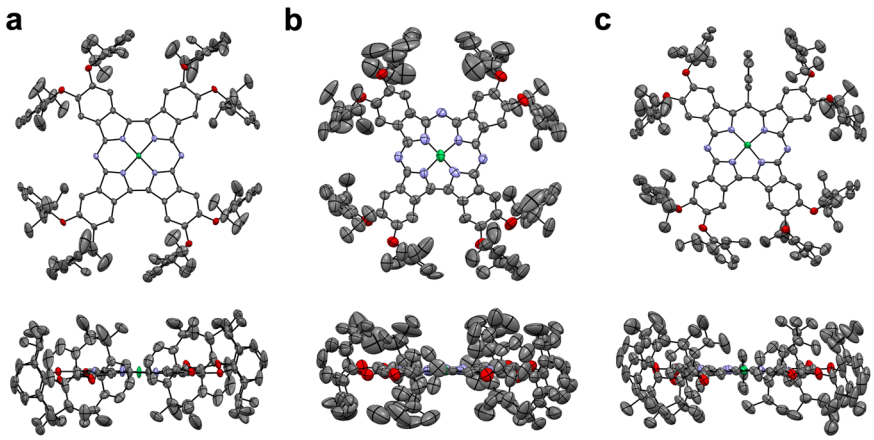

Fig. 3 | X-ray structures. Top and side views of (**a**) **2**, (**b**) **3**, and (**c**) **4**. One of the two molecules in the asymmetric unit is shown. Hydrogen atoms are omitted for clarity. Thermal ellipsoids are drawn at the 30% probability level. Carbon, nitrogen, oxygen, and nickel atoms are drawn in gray, blue, red, and green, respectively.

were estimated to be about +20 ppm, indicating the presence of distinct antiaromaticity. In contrast to **2**, diazacorrole derivatives **3** and **4** exhibited broad ^{1}H NMR signals in CD_2Cl_2 even at −90 °C (Supplementary Figs. 2, 4). The electron spin resonance (ESR) spectra of **3** and **4** in toluene at room temperature exhibited sharp signals at $g = 2.0048$ and 2.0039, respectively, indicating π-radical character instead of Ni-centered radical character (Fig. 4c, d)[28]. These ESR signals suggest that the oxidation state of Ni is not paramagnetic Ni(III) but diamagnetic Ni(II), which is similar to the case of Ni(II) corrole π-radicals[29–34]. The calculated spin density plots on radicals **3'** and **4'** without any peripheral substituents showed that the spin populations were delocalized over the azacorrole skeleton, consistent with the experimental ESR data (Supplementary Fig. 29).

Figure 5a shows the electronic absorption spectra of **2, 3**, and **4** in $CHCl_3$. The spectrum of macrocycle **2** showed a weak, broad, visible-near-IR absorption band tailing up to 1200 nm, which is different from the intense Q-bands usually observed for regular phthalocyanines[1]. This absorption of **2** is characteristic of 4$n\pi$-electron antiaromatic porphyrinoids, whose HOMO-LUMO transition is symmetry-forbidden[13,20]. **3** and **4** exhibited Q-like bands in the near-IR region at 770 nm ($\varepsilon = 8.37 \times 10^3\,M^{-1}\,cm^{-1}$) and 751 nm ($\varepsilon = 1.40 \times 10^4\,M^{-1}\,cm^{-1}$), respectively. Additionally, broad absorption peaks at 1431 nm ($\varepsilon = 6.40 \times 10^2\,M^{-1}\,cm^{-1}$) and 1193 nm ($\varepsilon = 6.98 \times 10^2\,M^{-1}\,cm^{-1}$) for **3** and at 1665 nm ($\varepsilon = 5.42 \times 10^2\,M^{-1}\,cm^{-1}$) and 1345 nm ($\varepsilon = 5.32 \times 10^2\,M^{-1}\,cm^{-1}$) for **4** are consistent with π-radical character[28]. These absorption bands of **3** and **4** span the second near-IR region (NIR-II, 1000–1700 nm), a desirable optical window for biological applications[35–39]. No detectable emission was observed for **2, 3**, or **4** in $CHCl_3$ at room temperature.

Cyclic voltammetry (CV) measurements of **2, 3**, and **4** were performed in CH_2Cl_2 to examine their redox potentials (Fig. 5b). **2** exhibited two reversible reduction peaks ($E_{1/2} = -1.11$ and −1.46 V vs Fc/Fc$^+$) in a narrow range, suggesting the facile conversion of 16π-electron antiaromaticity to 18π-electron aromaticity. An irreversible oxidation

https://doi.org/10.1038/s41467-025-58419-9

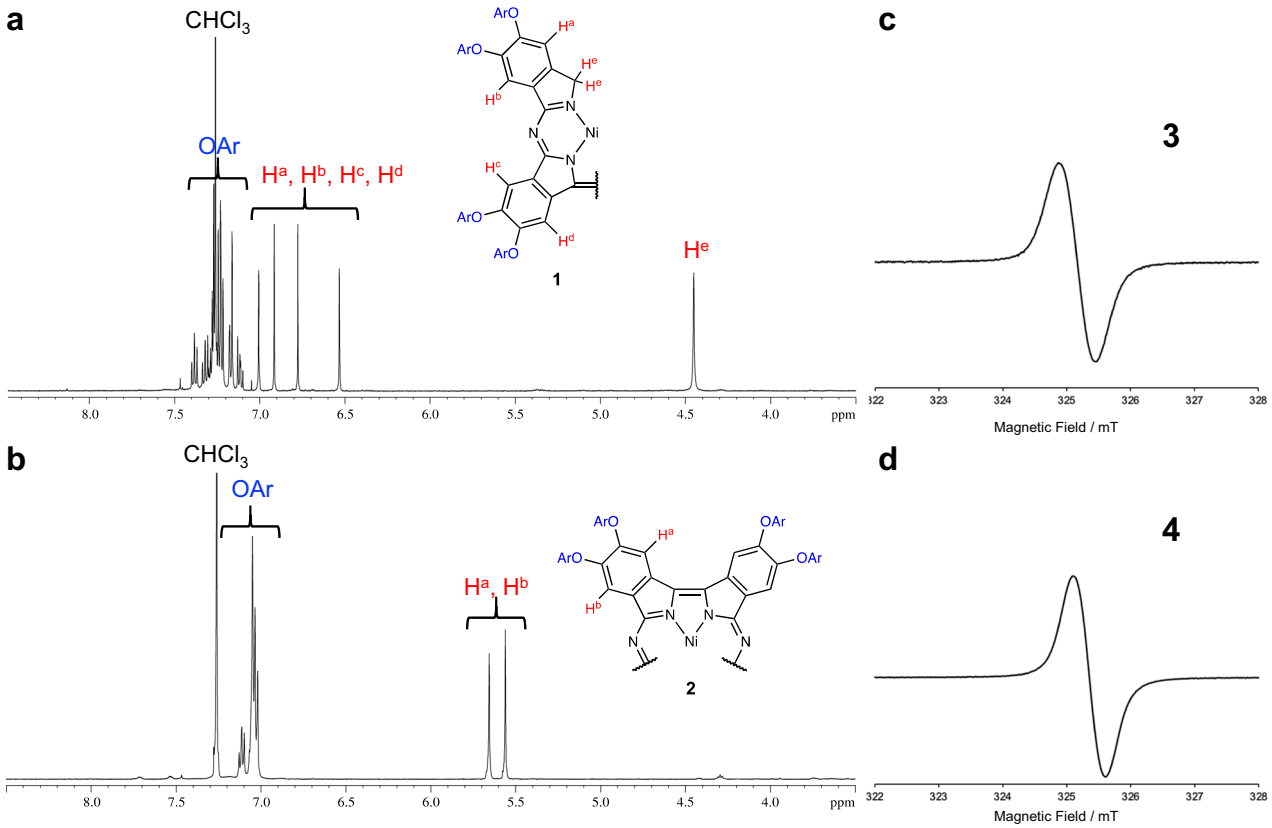

Fig. 4 | ^{1}H NMR and ESR spectra. Partial ^{1}H NMR spectra of (**a**) **1** and (**b**) **2** in $CDCl_3$ (500 MHz). ESR spectra of (**c**) **3** and (**d**) **4** in toluene (9125 MHz).

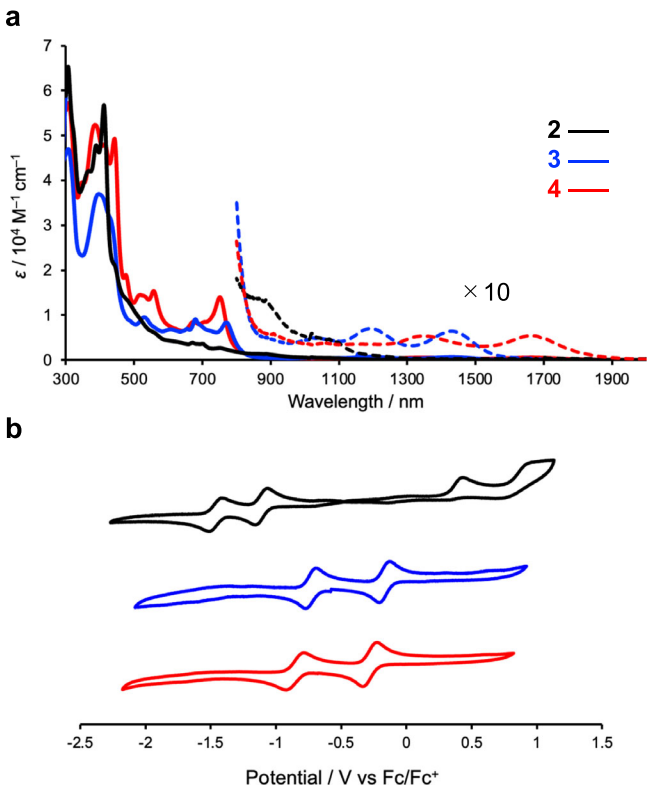

Fig. 5 | Physicochemical properties. a Electronic absorption spectra of **2** (black), **3** (blue), and **4** (red) in $CHCl_3$. **b** Cyclic voltammograms of **2** (black), **3** (blue), and **4** (red) in CH_2Cl_2.

wave was observed at $E_{ox,pa}$ = +0.43 V vs Fc/Fc$^+$. In contrast, π-radicals **3** and **4** both exhibited reversible reduction (**3**: $E_{1/2}$ = −0.73 V; **4**: $E_{1/2}$ = −0.85 V vs Fc/Fc$^+$) and oxidation waves (**3**: $E_{1/2}$ = −0.17 V; **4**: $E_{1/2}$ = −0.28 V vs Fc/Fc$^+$). The extremely narrow redox potential gaps (**3**: 0.56 V; **4**: 0.57 V) are consistent with the 17π-electron radical character of **3** and **4** owing to favorable single-electron transfer for both reduction and oxidation. These electrochemical characteristics of **3** and **4** are similar to those of the recently reported Ni tetrabenzocorrole π-radicals, which were easily converted to 16π-electron antiaromatic and 18π-electron aromatic species[31–33]. Therefore, oxidation and reduction of **3** and **4** by chemical reagents were investigated (Supplementary Information Section 2–4). Single-electron oxidation of **3** and **4** by $NO^+BF_4^-$ generated broad, weak near-IR absorption reminiscent of that of **2** (Supplementary Fig. 25). The ^{1}H NMR spectra showed upfield aromatic signals around 6 ppm, indicating the formation of 16π-electron antiaromatic species assigned as **3**$^+$ and **4**$^+$ (Supplementary Figs. 9, 11). In contrast, single-electron reduction of **3** and **4** by $CoCp_2$ led to the generation of sharp, strong red absorption reminiscent of the intense Q-bands observed for 18π-electron aromatic tetrabenzotriazacorrole (Supplementary Fig. 26)[25]. The ^{1}H NMR spectra displayed downfield aromatic signals around 8 ppm, indicating the formation of 18π-electron aromatic species assigned as **3**$^-$ and **4**$^-$ (Supplementary Figs. 10, 12). This is a marked feature of phthalocyanine-based structure, different from porphyrin analogs, which possess weak Q-bands.

To elucidate the origin of the observed optical and electrochemical properties of macrocycles **2, 3**, and **4**, we conducted frontier molecular orbital (FMO) analysis and time-dependent density functional theory (TD-DFT) calculation of model compounds **2', 3'**, and **4'** (Supplementary Information Section 4). The nodal patterns of the highest occupied molecular orbital (HOMO) and lowest unoccupied

https://doi.org/10.1038/s41467-025-58419-9

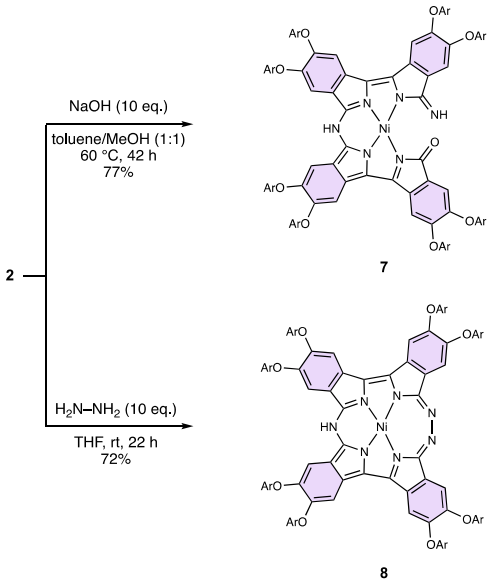

Fig. 6 | Skeletal transformation of 2. Synthesis of ring-opened compound **7** and ring-expanded macrocycle **8**.

molecular orbital (LUMO) of **2'** are similar to those of a pair of degenerate singly occupied and unoccupied molecular orbitals (SOMOs and SUMOs) in the 16π-electron perimeter model (Supplementary Fig. 30)[40,41], consistent with the experimentally observed antiaromaticity of **2**. However, tetrabenzodiazanorcorrole **2** exhibited a closed-shell character judging from its sharp signals observed in the ^{1}H NMR spectrum (Fig. 4b), in contrast to a reported 16π-electron antiaromatic tetrabenzonorcorrole, which has an open-shell, singlet diradical character[21]. We think that the difference is due to the larger HOMO-LUMO energy gap of **2** (1.49 V) (Fig. 5b, Supplementary Table 5) than that of tetrabenzonorcorrole (0.75 V)[21], which is attributable to the stabilization of the HOMO energy of **2** by the two electronegative nitrogen atoms at the *meso*-positions (Supplementary Fig. 30). Radical species **3'** and **4'** exhibited analogous FMOs localized mainly on the π-planes, although the energy levels of **3'** are slightly lower than those of **4'** due to the electronegative *meso*-nitrogen atom (Supplementary Figs. 31, 32). Their FMOs, i.e., α-SOMO−1s, α-SOMOs, β-SOMOs, and β-SUMOs, are related to a pair of degenerate SOMOs of the 16π-electron perimeter model[40,41], indicating that **3'** and **4'** have 17π-electron systems, similarly to the reported 17π-electron Ni tetrabenzocorrole π-radicals[31–33].

Transformation of macrocycle 2

Next, we considered further skeletal transformations of these phthalocyanine derivatives. Especially, 16π-electron macrocycle **2** was expected to show high reactivity owing to its antiaromaticity (Fig. 6). Treatment of **2** with NaOH afforded ring-opened nonaromatic compound **7**. Additionally, we found the reaction of **2** with hydrazine gave ring-expanded 18π-electron aromatic macrocycle **8**. The structures of **7** and **8** were confirmed by X-ray analysis (Supplementary Figs. 17, 18). The ^{1}H NMR spectra of **8** showed low-field shifts of isoindolinic α protons at 7.97–7.53 ppm (Supplementary Fig. 5), consistent with 18π-electron aromatic ring current effects. Compounds **7** and **8** exhibited stronger absorption bands in the red region around 650 nm than **2** (Supplementary Figs. 23, 24), reflecting the changes in aromaticity. These reactions of macrocycle **2** can be regarded as skeletal editing, which has recently attracted attention for the synthesis of small heterocycles[42,43].

In summary, we have developed a synthetic methodology for new phthalocyanine skeletons. Folding of linear tetramer **5** by Ni complexation, followed by deprotonative macrocyclization provides a strategy for the synthesis of *meso*-edited phthalocyanine derivatives as their Ni(II) complexes, exemplified here by tetrabenzodiazanorcorrole **2**, tetrabenzotriazacorrole **3**, and tetrabenzodiazacorrole **4**. These air-stable macrocycles exhibited striking physicochemical properties, such as 16π-electron antiaromaticity of **2** and 17π-electron radical character of **3** and **4**. Further, the antiaromatic macrocycle **2** was susceptible to nucleophilic cleavage, enabling skeletal transformations. We believe the current protocol opens up a versatile access to diverse phthalocyanine-like macrocycles. Efforts to expand the reaction scope, including access to the free-base[44] and variously metalated macrocycles, and to elucidate the reaction mechanisms with the help of theoretical and spectroscopic studies are in progress in our laboratory. We believe this approach is potentially applicable to the synthesis of a range of extended π-conjugated functional molecules, which are expected to have unique physicochemical properties.

Methods

Instrumentation

^{1}H and ^{13}C NMR spectra were obtained on a Bruker AVANCE NEO 500 spectrometer. Samples were recorded in $CDCl_3$, CD_2Cl_2, pyridine-d_5, DMSO-d_6, or THF-d_8. Chemical shifts are expressed in δ (ppm) values. ^{1}H spectra were referenced to tetramethylsilane (δ = 0.00 ppm), residual $CHCl_3$ (δ = 7.26 ppm), residual $CHDCl_2$ (δ = 5.32 ppm), residual pyridine-d_4 (δ = 8.74 ppm), residual DMSO-d_5 (δ = 2.50 ppm), or residual THF-d_7 (δ = 3.50 ppm) as an internal standard. ^{13}C spectra were referenced to tetramethylsilane (δ = 0.00 ppm) or $CDCl_3$ (δ = 77.16 ppm) as an internal standard. The following abbreviations are used: s = singlet, d = doublet, t = triplet, sept = septet, m = multiplet, br = broad. ESR spectra were obtained on a JEOL JES-X320 spectrometer. IR spectra were obtained on a JASCO FT/IR 4700 spectrometer. ESI-MS spectra were measured on a Bruker compact spectrometer. Ultraviolet-visible-near-IR absorption spectra were recorded with a JASCO V-770 spectrophotometer. Emission spectra were recorded on a JASCO FP-8750 spectrofluorometer. Cyclic voltammetry measurements were carried out with a Hokuto Denko HZ-110 voltammetric analyzer. Single crystal X-ray analysis was performed with a Rigaku XtaLAB Synergy-S diffractometer with a HyPix-6000HE HPC detector. All the reactions were performed under an Ar atmosphere using a standard Schlenk technique or an Ar glovebox (MBRAUN, Labmaster Pro).

Materials

Materials were purchased from Merck-Sigma-Aldrich Corporation, FUJIFILM Wako Pure Chemical Corporation, Tokyo Chemical Industry Corporation, and Kanto Chemical Corporation. Dehydrated toluene, CH_2Cl_2, and tetrahydrofuran (THF) were purchased from Kanto Chemical and purified by a solvent purification system of Glass-Contour. Flash column chromatographic separation was performed with Yamazen medium pressure liquid chromatography (MPLC) system (EPCLC-W-Prep 2XY A-Type) using a disposable Hi-flash column from Yamazen Co. Merck Kiesel gel 60 F_{254} plate (0.25 mm thickness, coated on glass 20 × 20 cm^2) was used for analytical thin layer chromatography (TLC).

Data availability

The experimental and computational data generated in this study are provided in the article and the Supplementary Information, and also are available from the corresponding authors upon request. Source Data for the cartesian coordinates of the calculated structures are provided with this manuscript. Crystallographic data for the structures reported in this Article have been deposited at the Cambridge Crystallographic Data Centre, under deposition numbers CCDC 2382224 (**1**), 2382225 (**2**), 2382226 (**3**), 2382227 (**4**), 2416449 (**7**), and 2382228 (**8**). Copies of the data can be obtained free of charge https://www.ccdc.cam.ac.uk/structures/. Source data are provided with this paper.

References

1. McKeown, N. B. *Phthalocyanine Materials: Synthesis, Structure and Function* (Cambridge University Press, Cambridge, 1998).
2. Janczak, J. & Kubiak, R. Gadolinium(III) bicyclic phthalocyanine. *Acta. Cryst* **C51**, 2039–2042 (1995).
3. Claessens, C. G., González-Rodríguez, D. & Torres, T. Subphthalocyanines: singular nonplanar aromatic compounds–synthesis, reactivity, and physical properties. *Chem. Rev.* **102**, 835–854 (2002).
4. Mack, J. & Kobayashi, N. Low symmetry phthalocyanines and their analogues. *Chem. Rev.* **111**, 281–321 (2011).
5. Yamamoto, S., Dudkin, S. V., Kimura, M. & Kobayashi, N. Phthalocyanine synthesis. in *Handbook of Porphyrin Science* Vol. 45 (eds. Kadish, K. M., Smith, K. M. & Guilard, R.) 1–168 (World Scientific Publishing, 2019).
6. Urbani, M., Ragoussi, M.-E., Nazeeruddin, M. K. & Torres, T. Phthalocyanines for dye-sensitized solar cells. *Coord. Chem. Rev.* **381**, 1–64 (2019).
7. Zheng, B.-D., He, Q.-X., Li, X., Yoon, J. & Huang, J.-D. Phthalocyanines as contrast agents for photothermal therapy. *Coord. Chem. Rev.* **426**, 213548 (2021).
8. Niyas, M. A., Shoyama, K. & Würthner, F. C_{64} Nanographene tetraimide—a receptor for phthalocyanines with subnanomolar affinity. *Angew. Chem. Int. Ed.* **62**, e202302032 (2023).
9. Lash, T. J. Carbaporphyrinoid systems. *Chem. Rev.* **117**, 2313–2446 (2017).
10. Orłowski, R., Gryko, D. & Gryko, D. T. Synthesis of corroles and their heteroanalogs. *Chem. Rev.* **117**, 3102–3137 (2017).
11. Senge, M. O., Sergeeva, N. N. & Hale, K. J. Classic highlights in porphyrin and porphyrinoid total synthesis and biosynthesis. *Chem. Soc. Rev.* **50**, 4730–4789 (2021).
12. Toganoh, M. & Furuta, H. Creation from confusion and fusion in the porphyrin world—the last three decades of N-confused porphyrinoid chemistry. *Chem. Rev.* **122**, 8313–8437 (2022).
13. Furuyama, T., Sato, T. & Kobayashi, N. A bottom-up synthesis of antiaromatic expanded phthalocyanines: Pentabenzotriazasmaragdyrins, i.e. Norcorroles of superphthalocyanines. *J. Am. Chem. Soc.* **137**, 13788–13791 (2015).
14. Xu, Y. et al. Helical β-isoindigo-based chromophores with B–O–B bridge: facile synthesis and tunable near-infrared circularly polarized luminescence. *Angew. Chem. Int. Ed.* **62**, e202218023 (2023).
15. Zhu, L. & Ng, D. K. P. Synthesis of a β-isoindigo-linked 1*H*-3-benzazepine-modified aza-boron dipyrromethene dimer. *Arkivoc* **(ii)**, 202312022 (2023).
16. Zhang, Y. et al. Novel, linear oligoisoindole compounds with a conjugated electronic structure. *Org. Chem. Front.* **4**, 2364–2369 (2017).
17. Zatsikha, Y. V., Shamova, L. I., Herbert, D. E. & Nemykin, V. N. β-Isoindigo-azaDIPYs: fully conjugated hybrid systems with broad absorption in the visible region. *Angew. Chem. Int. Ed.* **60**, 12304–12307 (2021).
18. Cordero, B. et al. Covalent radii revisited. *Dalton Trans* **7**, 2832–2838 (2008).
19. Bröring, M., Köhler, S. & Kleeberg, C. Norcorrole: observation of the smallest porphyrin variant with a N_4 core. *Angew. Chem. Int. Ed.* **47**, 5658–5660 (2008).
20. Ito, T. et al. Gram-scale synthesis of nickel (II) norcorrole: the smallest antiaromatic porphyrinoid. *Angew. Chem. Int. Ed.* **51**, 8542–8545 (2012).
21. Yoshida, T. et al. Benzonorcorrole Ni^{II} complexes: enhancement of paratropic ring current and singlet diradical character by benzofusion. *Angew. Chem. Int. Ed.* **57**, 2209–2213 (2018).
22. Kino, S. et al. Close stacking of antiaromatic Ni (II) norcorrole originating from a four-electron multicentered bonding interaction. *J. Am. Chem. Soc.* **146**, 9311–9317 (2024).
23. Fujiki, M., Tabei, H. & Isa, K. New tetrapyrrolic macrocycle: α,*β*,γ-triazatetrabenzcorrole. *J. Am. Chem. Soc.* **108**, 1532–1536 (1986).
24. Li, J., Subramanian, L. R., Hanack, M. Substituted α,β,γ-triazatetrabenzcorrole: an unusual reduction product of a phthalocyanine. *Chem. Commun*. 679–680 (1997).
25. Zhang, X.-F. Tetrabenzotriazacorrole: Its synthesis, reactivity, physical properties, and applications. *Coord. Chem. Rev.* **285**, 52–64 (2015).
26. Takahashi, Y. et al. Charge conduction properties at the contact interface between (Phthalocyaninato)nickel(II) and electron acceptor single crystals. *Chem. Mater.* **26**, 993–998 (2014).
27. Schleyer, Pv. R., Maerker, C., Dransfeld, A., Jiao, H. & Hommes, N. J. Rv. E. Nucleus-independent chemical shifts: a simple and efficient aromaticity probe. *J. Am. Chem. Soc.* **118**, 6317–6318 (1996).
28. Shimizu, D. & Osuka, A. Porphyrinoids as a platform of stable radicals. *Chem. Sci.* **9**, 1408–1423 (2018).
29. Will, S. et al. Nickel and copper corroles: well-known complexes in a new light. *Angew. Chem. Int. Ed.* **36**, 357–361 (1997).
30. Ghosh, A., Wondimagegn, T. & Parusel, A. B. J. Electronic structure of gallium, copper, and nickel complexes of corrole. high-valent transition metal centers versus noninnocent ligands. *J. Am. Chem. Soc.* **122**, 5100–5104 (2000).
31. Gao, H. et al. Highly stable neutral corrole radical: amphoteric aromatic–antiaromatic switching and efficient photothermal conversion. *J. Am. Chem. Soc.* **144**, 3458–3467 (2022).
32. Gao, H., Wu, F., Zhao, Y., Yang, X. & Shen, Z. Redox-switchable bistable nickel corrole. *Inorg. Chem. Front.* **10**, 3037–3046 (2023).
33. Gao, H. et al. Molecular engineering of corrole radicals by polycyclic aromatic fusion: towards open-shell near-infrared materials for efficient photothermal therapy. *Angew. Chem. Int. Ed.* **62**, e202309208 (2023).
34. Gao, H., Wu, F., Wang, K. & Shen, Z. Recent developments in corrole radicals. *J. Porphyrins Phthalocyanines* **27**, 946–957 (2023).
35. Kenry, Duan, Y. & Liu, B. Recent advances of optical imaging in the second near-infrared window. *Adv. Mater.* **30**, 1802394 (2018).
36. Levaud, L. et al. Fused bis-azacalixphyrin that reaches NIR-II absorptions. *Chem. Commun.* **56**, 896–899 (2020).
37. Mu, J. et al. The chemistry of organic contrast agents in the NIR-II window. *Angew. Chem. Int. Ed.* **61**, e202114722 (2022).
38. Li, C. et al. Rationally designed Ru(II)-metallacycle chemophototheranostic that emits beyond 1000 nm. *Chem. Sci.* **13**, 6541–6549 (2022).
39. Yanagi, S. et al. 20π-electron antiaromatic Benziphthalocyanines with absorption reaching the near-infrared-II region. *Chem. Eur. J.* **30**, e202400401 (2024).
40. Höweler, U., Downing, J. W., Fleischhauer, J. & Michl, J. MCD of nonaromatic cyclic π-electron systems. Part 1. The perimeter model for antiaromatic 4*N*-electron [*n*]annulene biradicals[1]. *J. Chem. Soc. Perkin Trans.* **2**, 1101–1108 (1998).
41. Fleischhauer, J., Höweler, U. & Michl, J. MCD of Nonaromatic Cyclic *π*-Electron Systems. 3.[1] The Perimeter Model for Low-Symmetry "Unaromatic" and "Ambiaromatic" Molecules Derived from 4*N*-Electron [*n*]Annulenes. *J. Phys. Chem. A* **104**, 7762–7775 (2000).
42. Jurczyk, J. et al. Single-atom logic for heterocycle editing. *Nature Synthesis* **1**, 352–364 (2022).
43. Joynson, B. W. & Ball, L. T. Skeletal editing: interconversion of arenes and heteroarenes. *Helv. Chim. Acta* **106**, e202200182 (2023).
44. Liu, L. et al. Synthesis of subporphyrin free bases. *Angew. Chem. Int. Ed.* **61**, e202214342 (2022).

Acknowledgements

We thank Dr. Takashi Kikuchi (Rigaku Corporation) for the support of single-crystal X-ray diffraction analysis of compound **8**. We also thank Dr. Yukio Mizuta and Dr. Aiko Shimada (JEOL Ltd.) for the support with ESR measurements of compounds **3** and **4**. This work was supported in

part by grants from JSPS KAKENHI (A) (No. 22H00320), JST CREST (No. JPMJCR19R2), NAGASE Science Technology Foundation, Naito Foundation, Chugai Foundation, Uehara Memorial Foundation (to M.U.), Mochida Memorial Foundation, Uehara Memorial Foundation, Asahi Glass Foundation, JSPS KAKENHI for Young Scientists (No. 22K15245), and JSPS KAKENHI (B) (No. 24K02142) (to N.T.).

Author contributions

N.T. and M.U. conceived the work and designed, advised, and directed the project. Y.T., T.S., and N.T. conducted the experiments and analyzed the data. Y.T. and N.T. performed the computational calculations. N.T. and M.U. co-wrote the manuscript. All authors contributed to discussion.

Competing interests

The authors declare no competing interests.

Additional information

Supplementary information The online version contains supplementary material available at https://doi.org/10.1038/s41467-025-58419-9.

Correspondence and requests for materials should be addressed to Naoyuki Toriumi or Masanobu Uchiyama.

Peer review information *Nature Communications* thanks the anonymous reviewer(s) for their contribution to the peer review of this work. A peer review file is available.